Biophysical Chemistry 180–181 (2013) 1–9

Contents lists available at ScienceDirect

Biophysical Chemistry

journal homepage: http://www.elsevier.com/locate/biophyschem

Molecular dynamics investigation of Cl^- transport through the closed and open states of the $2\alpha_1 2\beta_2\gamma_2$ $GABA_A$ receptor

Hong-Bo Xie, Jian Wang, Yu Sha *, Mao-Sheng Cheng **

Key Laboratory of Structure-Based Drugs Design & Discovery of Ministry of Education, School of Pharmaceutical Engineering, Shenyang Pharmaceutical University, Shenyang 110016, PR China

HIGHLIGHTS

- Homology models are embedded into a lipid bilayer to perform MD simulation.
- Some structural features of the GABAAR are explored by performing MD simulations.
- ABF simulation is used to evaluate the energy barriers for the Cl— permeation.

GRAPHICAL ABSTRACT

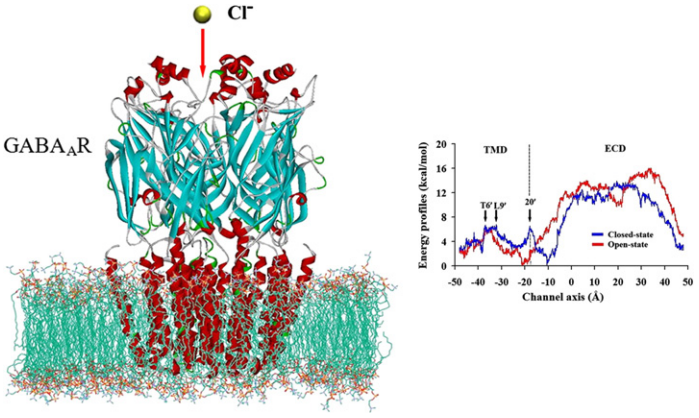

ARTICLE INFO

Article history:
Received 1 March 2013
Received in revised form 18 May 2013
Accepted 20 May 2013
Available online 26 May 2013

Keywords:
Gamma-aminobutyric type A receptor ($GABA_AR$)
Homology modeling
Molecular dynamics (MD) simulation
Adaptive biasing force (ABF)

ABSTRACT

The $\alpha_1\beta_2\gamma_2$ gamma-aminobutyric type A receptor ($GABA_AR$) is one of the most widely expressed $GABA_AR$ subtypes in the mammalian brain. $GABA_ARs$ belonging to the Cys-loop superfamily of ligand-gated ion channels have been identified as key targets for many clinical drugs, and the motions that govern the gating mechanism are still not well understood. In this study, an open-state $GABA_AR$ was constructed using the structure of the glutamate-gated chloride channel (GluCl), which has a high sequence identity to $GABA_AR$. A closed-state model was constructed using the structure of the nicotinic acetylcholine receptor (nAChR). Molecular dynamics simulations of the open-state and closed-state $GABA_AR$ were performed. We calculated the electrostatic potential of the two conformations, the pore radius of the two ion channels and the root-mean-square fluctuation. We observed the presence of two positively charged girdles around the ion channel and found flexible regions in the $GABA_AR$. Then, the free-energy of chloride ion permeations through the closed-state and open-state $GABA_AR$ has been estimated using adaptive biasing force (ABF) simulation. For the closed-state $GABA_AR$, we observed two major energy barriers for chloride ion translocation in the transmembrane domain (TMD). For the open-state $GABA_AR$, there was only one energy barrier formed by two Thr261 (α_1), two Thr255 (β_2) and one Thr271 (γ_2). By using ABF simulation, the overall free-energy profile is obtained for Cl^- transporting through $GABA_AR$, which gives a complete map of the ion channel of Cl^- permeation.

* Corresponding author. Tel.: +86 24 23986415; fax: +86 24 23995043.
** Corresponding author. Tel.: +86 24 23986413; fax: +86 24 23995043.
E-mail addresses: shayu@syphu.edu.cn (Y. Sha), mscheng@syphu.edu.cn (M.-S. Cheng).

0301-4622/$ – see front matter © 2013 Elsevier B.V. All rights reserved.
http://dx.doi.org/10.1016/j.bpc.2013.05.004

1. Introduction

Gamma-aminobutyric acid type A receptors ($GABA_ARs$) are the major inhibitory neurotransmitter receptors in the central nervous system and can be modulated by a variety of pharmacologically and clinically important drugs [1–3]. $GABA_ARs$ belong to the Cys-loop superfamily of ligand-gated ion channels, which can rapidly mediate synaptic signal transduction throughout the nervous system. Other members of this family include the nicotinic acetylcholine receptor (nAChR), the serotonin receptor ($5\text{-}HT_3R$) and the strychnine-sensitive glycine receptor (GlyR) [4]. Previous studies have shown that, as therapeutic targets, the $GABA_ARs$ are of critical physiological importance and their malfunctions are related to a number of known diseases including anxiety, schizophrenia, sleeplessness and epilepsy [5,6].

The $GABA_ARs$ are membrane-bound proteins that may be assembled from at least 19 subunits belonging to eight different classes (6α, 3β, 3γ, 1δ, 1ε, 1θ, 1π and 3ρ) [7–10]. All of these subunits can form functional heteropentameric receptors with central ion-conducting pores. The majority of native $GABA_ARs$ seem to be composed of two α, two β and one γ subunit, and the most abundant subtype is $2\alpha_1 2\beta_2\gamma_2$. The structure of each subunit can be subdivided into three domains: the extracellular domain (ECD), four transmembrane domains (TM_1–TM_4), with TM_2 lining the pore of the channel, and a cytoplasmic loop of variable length that links TM_3 and TM_4.

Thus far, many clinical drugs for the $GABA_ARs$ have been exploited to treat various central nervous system diseases. However, little detailed information about the ion channel gating mechanism is known due to the absence of high-resolution structures of the $GABA_ARs$. To the best of our knowledge, many groups have published homology models of the $GABA_ARs$. Most of these models only reconstructed the ECD to predict how ligands bind to binding sites or to test the binding affinities of novel ligands [11–14]. However, many aspects of the $GABA_AR$ remain poorly understood. Compared to numerous modeling analyses of ligand docking, few theoretical modeling studies were focused on the structural properties of the $GABA_ARs$. What happens to the structural conformation and the electrostatic potential as ligands bind to the protein? Which residues in the central pore may act to block ion permeation? How can the receptor achieve ion selectivity? There are still no general answers to these questions. Indeed, to answer these questions, we must learn about the specific changes in different states of the protein. To date, an increasing number of studies have discussed the differences between the diverse conformations of ligand-gated ion channels [15,16].

At present, utilizing simple "brute force" MD simulations to study ion permeation remains computationally prohibitive, as the time-scale to observe the translocation of ions is on the order of a typical MD trajectory. To avoid these difficulties, people can compute the free energy profile or potential of mean force (PMF), governing the elementary microscopic steps of ion translocation in the pore [17]. A practicable approach is the adaptive biasing force (ABF) method, which estimates the PMF along the reaction coordinate by averaging the instantaneous force and canceling it by an adaptive biasing force [18–20]. For a biasing force that corresponds exactly to the PMF, the reaction coordinate has a purely diffusive motion. Another approach to compute the PMF is the "umbrella sampling" technique [21]. In this method, the investigated system is simulated in the presence of an artificial biasing window potential. To obtain the complete PMF, the data from several windows have to be combined together and the bias introduced by the constraining potentials has to be removed. Indeed, calculations of ion PMF in many ion channels have been reported [22–25].

In this study, we aimed to gain further information about the $\alpha_1\beta_2\gamma_2$ subtype $GABA_AR$ by running MD simulations with two conformations of the protein. Two homology models (closed-state and open-state) of the human $\alpha_1\beta_2\gamma_2$ $GABA_AR$ were generated. The quality of the modeled structures was evaluated using Ramachandran plots to ensure their validity for further studies. Then, the homology model was embedded into a lipid bilayer to perform a MD simulation. The root-mean-square deviation (RMSD) result showed that the two structures of the $\alpha_1\beta_2\gamma_2$ $GABA_AR$ ultimately became stable. After performing the simulations, we observed the changes in the structure conformation, electrostatic potential, and the radius of the ion pore. We determined an accurate single-ion PMF along the pore axis for each state model, which gave rise to the energetic barrier for Cl^- permeation. We aimed to get a comprehensive physical picture for the Cl^- permeation including the exact residues interacted with Cl^-, the changes of Cl^- PMF, and the differences between closed-state and open-state $GABA_AR$ for energy barriers. ABF simulation provides the most suitable approach for this purpose because it can get a detailed account of the changes occurring in the ion channel system during the ion flux process. Finally, we found two energy barriers in the closed-state $GABA_AR$ and one energy barrier in the open-state model. As the two models made predictions about the relative spatial positioning of residues, they permit the design of more specific mutagenesis experiments on the $GABA_ARs$. Comparing the changes of energy barriers, we provided new insights of the Cl^- ion transport mechanism.

2. Methods

The preparation, visualization and analysis of the homology modeling, MD simulation and ABF simulation were performed on a Dell PowerEdge R900 Server with Intel Xeon X7460 processors.

2.1. Homology modeling

The sequences of the human $GABA_AR$ α_1 (UniProt ID: P14867), β_2 (UniProt ID: P47870) and γ_2 (UniProt ID: P18507) subunits were retrieved from the ExPASy Molecular Biology Server (http://us.expasy.org). All three sequences were edited to remove the signal peptides and the long cytoplasmic loops of the intracellular domain (ICD). Template selection is an important starting point in homology modeling because it directly influences the quality of the target structure. Recently, Hibbs and Gouaux presented the first three-dimensional structure of an inhibitory anion-selective glutamate-gated chloride channel (GluCl) (PDB ID: 3RHW), which shares a high sequence identity (33.9%) with $GABA_AR$ [26]. GluCl is certainly a good template for the homology of open-state $GABA_AR$ because the structure of the GluCl was activated by binding ivermecine. $GABA_AR$ is also an anion-selective channel, so GluCl is a suitable template. We choose the nAChR from *Torpedo marmorata* (PDB ID: 2BG9) to model the closed-state $GABA_AR$. Although the sequence identity between $GABA_AR$ subunits and nAChR subunits is 24%, there is evidence to indicate that it is credible to use nAChR as template because they are both the members of the Cys loop ligand-gated ion channel superfamily [4,27,28].

The sequences of the α_1, β_2 and γ_2 subunits were aligned to the corresponding subunits of the template, which were implemented using the Align Sequences protocol within Discovery Studio 3.0 software package (Accelrys Inc.). We constructed the disulfide bonds in the α_1 (Cys139–Cys153), β_2 (Cys135–Cys149) and γ_2 (Cys151–Cys165) subunits. For each state, 20 homology models were built and scored by the Discrete Optimized Protein Energy (DOPE) method [29]. The structure with the lowest DOPE value was chosen for further study. Two theoretical $2\alpha_1 2\beta_2\gamma_2$-type arrangements have the one α_1–γ_2 and two α_1–β_2 subunit contacts necessary for the assumed benzodiazepine and GABA binding sites. Only one of these arrangements was well accepted and thus chosen for our study, which is shown in Fig. 1. Sigel et al. previously demonstrated the absolute arrangement of the $\alpha_1\beta_2\gamma_2$ $GABA_AR$ [30]. In the closed-state $GABA_AR$, because the template was formed with three different subunits, we choose a commonly accepted assembly method to model the pentameric receptor, which had been used in previous studies [11,12]. A schematic representation of the subunit correspondence between nAChR and the closed-state $GABA_AR$ is shown in Fig. 1. The subunits of the open-state and the closed-state models were both arranged in the same way. The quality

of the constructed models was assessed utilizing the Rampage server (http://www-cryst.bioc.cam.ac.uk) [31].

2.2. Regular MD simulations

Here, we describe two MD simulation systems. The simulation time was 15 ns each for the open-state and closed-state $GABA_AR$. The simulations were performed using the NAMD 2.8 program and the CHARMM27 force field with CMAP corrections was used for protein, water, and lipids [32,33]. The systems, simulated under constant 1 atm pressure, 310 K temperature and the NPT (constant number of atoms, pressure and temperature) ensemble, were regulated via Langevin piston pressure control and Langevin damping dynamics [34]. Periodic boundary conditions and water wrapping were applied. The bonded interactions and the short-range non-bonded interactions were calculated at every time-step (2 fs) and every two time-steps, respectively. Using the particle mesh Ewald method [35], we calculated the long-range electrostatic interactions at every four time-steps. PMEGridSpacing was set 1.0 Å. The cutoff distance for non-bonded interactions was 12 Å. A smoothing function was employed for the van der Waals interactions at a distance of 10 Å. A pair list of the non-bonded interactions was calculated using a pair distance of 14 Å. We embedded the built ion channel into the center of a 130 Å × 130 Å fully hydrated 1-Palmitoyl-2-Oleoyl-sn-Glycero-3-Phosphatidylcholine (POPC) lipid, and all overlapping lipids and water molecules were removed. Then, the system was fully solvated to a box size of 140 Å × 140 Å × 140 Å with TIP3P water molecules, Na^+ and Cl^- to neutralize the overall charge and obtain a final ion concentration of 0.15 M. There were one $GABA_AR$, 301 POPC, 111 Cl^- ions, 95 Na^+ ions, and about 88,500 water molecules for a total of over 333,000 atoms.

2.3. ABF simulations

The single ion PMF for Cl^- transporting through the open-state and closed-state $GABA_AR$ was calculated using the ABF simulation. The method couples ideas from thermodynamic integration and average force formalisms with unconstrained molecular dynamics and the introduction of an adaptive biasing potential. Briefly, a predefined intuitive coordinate ξ has to be selected. The average force experienced by the simulated system at any point along this coordinate is estimated from the instantaneous forces experienced by the system at that position. The average forces are accumulated in bins along ξ and are continuously updated as the simulation progresses. The estimated free energy derivative, computed for small intervals of ξ, is canceled by the introduction of an adaptive biasing potential. The application of the adaptive bias allows the system to overcome existing barriers along ξ in the free energy landscape. Error in adaptive biasing force method can be estimated by

$$\mathrm{SD}\left[\Delta A^{(abf)}\right] \approx (\xi_b - \xi_a)\frac{\sigma}{K^{1/2}}(1+2\kappa)^{1/2} \quad (1)$$

where $\Delta A^{(abf)}$ is the Adaptive biasing force estimate of the free energy, and K is the total number of molecular dynamics steps used to estimate $\Delta A^{(abf)}$. For large K the bin size can be made sufficiently small that the quadrature error becomes negligibly small. ξ is the generalized coordinate, F_ξ is the effective force acting on ξ, $\sigma^2 = \mathrm{Var}[F_\xi]$. And κ is the correlation length of the series $\{F_\xi(t_m)\}^K_{m=1}$. From this equation it follows that the standard deviation of $\Delta A^{(abf)}$ decreases as $K^{-1/2}$ and increases linearly with σ [36].

Additionally, the two structures were still embedded in POPC lipid bilayer over the course of Cl^- permeation. It permitted that the transmembrane domain (TMD) was maintained in the condition of membrane. In our case, the reaction coordinate is the channel permeation pathway, which is parallel to the bilayer normal (z direction). The simulations were carried out in 48 windows of length 2 Å along the z direction for each system. The reaction pathway extended to 96 Å and was sufficient to cover the entire length of the ECD and the TMD. The Langevin dynamics was employed to maintain the temperature at 310 K, and the Langevin piston method was used to maintain the pressure at 1 atm [34]. Periodic boundary conditions were applied in all directions. Within each window the average force acting on the selected ion was accumulated in 0.1 Å sized bins. Harmonic restraints (with force constant of 3 kcal/mol/Å^2) were applied to the protein C_α atoms. It should be emphasized that these restraints are not coupled to the reaction coordinate through common atoms so that the corresponding forces have no direct influence on the PMF calculation. 1 ns of trajectory was generated for each window, resulting in a total simulation time of 53 ns for open-state (5 windows in TMD simulated 2 ns) and 48 ns for closed-state $GABA_AR$.

3. Results and discussion

3.1. Validation of the homology models

The homology models were validated using the Rampage server. In the open-state model, 95.5% of the residues were found in the favored regions of the Ramachandran plot and 4% of the residues reside in the accepted regions. In the closed-state model, 93.5% of the residues fell in the favored regions and 5.2% of the residues reside in accepted regions (Fig. 2). It suggested that both of the homology model structures had satisfactory geometry and could be used for further MD simulation and ABF simulation studies. The template used to model the open-state $GABA_AR$ was GluCl. It had a high sequence identity to $GABA_AR$, especially in loop B, loop E, TM_1 and TM_2, as shown in Fig. 3. Furthermore, the TM_2 plays an important role in channel conductance and gating. Several key residues were identified with site-specific mutagenesis experiments, including Ser267 (γ_2), Thr261 (α_1), Ser272 (α_1) and Thr255 (β_2) [37,38]. In $GABA_AR$, TM_2 formed the pathway for ion translocation through the ion channel and played an important role in channel conductance and gating. And a residue numbering convention was established for TM_2 for comparison of sequence positions in $GABA_AR$, where $-1'$ designated the cytoplasmic end of TM_2 and $20'$ designated the extracellular end. Therefore, it is significant for studying $GABA_AR$ to model reliable TM_2. In our models, these key residues were all lining the pore of the channel, which also demonstrated that the two homology models had satisfactory geometry.

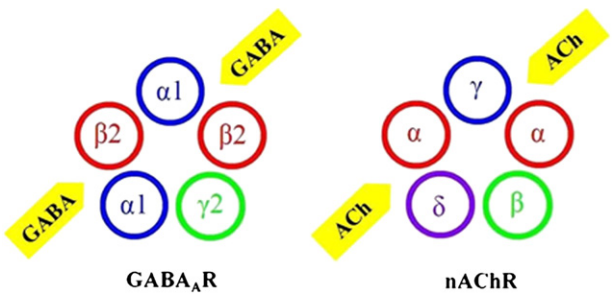

Fig. 1. The view from the synaptic cleft shows the absolute subunit arrangements of the $\alpha_1\beta_2\gamma_2$ $GABA_AR$ and the nAChR. The ACh and GABA binding sites are indicated by arrows.

3.2. Regular MD simulations

The overall stabilities of the closed and open channel structures were evaluated using the RMSD of the backbone atoms from their initial homology model positions (Fig. 4). The closed-state model reached a stable stage after 10 ns of the simulation, with an average RMSD value of approximately 4.25 Å. The overall RMSD of the open-state model after a 15-ns MD simulation was 3.5 Å. These results suggested that both the experimental structures achieved stable in our simulation protocol.

It should be noted that the receptor channel exists in at least three different conformations: open, closed and desensitized. Open-state receptor could bind with agonist and is activated. If no agonists are bound to the receptor and the receptor is not activated, it will stay in the closed state. Desensitization is a general characteristic of ligand-gated channels, whereby a decrease or loss of biological response occurs following prolonged or repetitive stimulation. Despite the conversion to a high-affinity state, desensitization results in decreased responsiveness of the receptor for a subsequent stimulus. In the present study, pore radius calculations were performed using the HOLE program [39]. The results show that the closed-state and open-state $GABA_AR$s both became narrower after 15 ns simulations, as shown in Fig. 5. This change is even clearer in the open-state model than the closed-state model, because the open channel tends to be constricted when no ligand is bound. However, the simulation time was not sufficient to complete the full conversion, so the model remained in open state. In the simulation system of closed-state model, the pore-radius changed not much because it was still in the closed state under the non-ligand-bound condition. In all, the pore radius of the channel decreased over the MD simulation. This decrease was especially obvious in the TMD, which indicated that this region has the potential to become constricted. Although the pore of the ion channel became narrower, the pore radius was still large enough to accommodate water molecules or Cl^-.

In addition, Poisson Boltzmann electrostatics calculations for the two models were carried out using the APBS [40] package. The charge and radius parameters for APBS were assigned using PDB2PQR [41]. The electrostatic potential (ESP) profiles of the channel from APBS calculations for the two models are shown in Fig. S1–S2. Notably, throughout the MD simulation, in both the closed-state and open-state models, the entrance of the ECD and the end of the TMD were highly positively charged. To locate the flexible regions of the two models, the root-mean-square fluctuation (RMSF) was calculated and plotted for the C_α atoms over the last 5 ns of the simulations. The RMSF plots for all subunits of the two models are provided in Fig. S3. Clearly, in each subunit, the N-terminal domain was comparatively more flexible. In addition, several loops in the subunits of this domain showed greater conformational flexibility.

3.3. ABF simulations

Using the ABF method, we presented the 1D PMF for transporting one Cl^- along the channel centerline in the two systems. Fig. 6 shows the PMFs for transporting Cl^- through the closed-state and open-state $GABA_AR$. The major energy barrier appeared in the ECD with 13 ± 0.5 kcal/mol in the closed-state $GABA_AR$. The same energy barrier with 14 ± 0.5 kcal/mol appeared in open-state $GABA_AR$, which demonstrated the region is a gate of the Cl^- permeation. In the study of a cation-selective open-state GLIC, Tang et al. found a significant Na^+ energy barrier in the ECD [42]. They proposed that the unique phenomenon was due to the protonation of several acidic residues in this region and the lower channel conductance than other GLIC. In contrast, as $GABA_AR$ is an anion channel, we inferred that the energy barrier for Cl^- in the ECD of $GABA_AR$ was due to basic residues (positively charged residues) in this region. We analyzed the residues with the highest energy barriers, more precisely, at the loop A, there are several key basic residues, including His110 (α_1), His106 (β_2), His122 (γ_2), Lys106 (α_1), Lys102 (β_2) and Lys118 (γ_2). It was recently found that single-channel conductance can also be influenced by residues in the ECD of the $GABA_AR$. Sivilotti et al. demonstrated that the positively charged residues (basic residues) in this region might boost the conductance of anionic Cys-loop channels [43]. Charge reversal mutations of Lys106 (α_1), Lys102 (β_2) and Lys118 (γ_2) produced a great decrease on outward conductance, which shows that these positively charged residues contribute to determine the rate of ion flow through $GABA_AR$.

In our study, more attention was focused on the PMF in the TMD than that in the ECD, because previous studies have implicated that TM_2 domains form the gating structures of the $GABA_AR$s [37,44,45]. In the TMD of the closed-state $GABA_AR$, two energy barriers of equal height (6.6 ± 0.2 kcal/mol) were found for Cl^-. The first one is near the residues of Asn275 (α_1), Glu269 (β_2) and Lys285 (γ_2). These

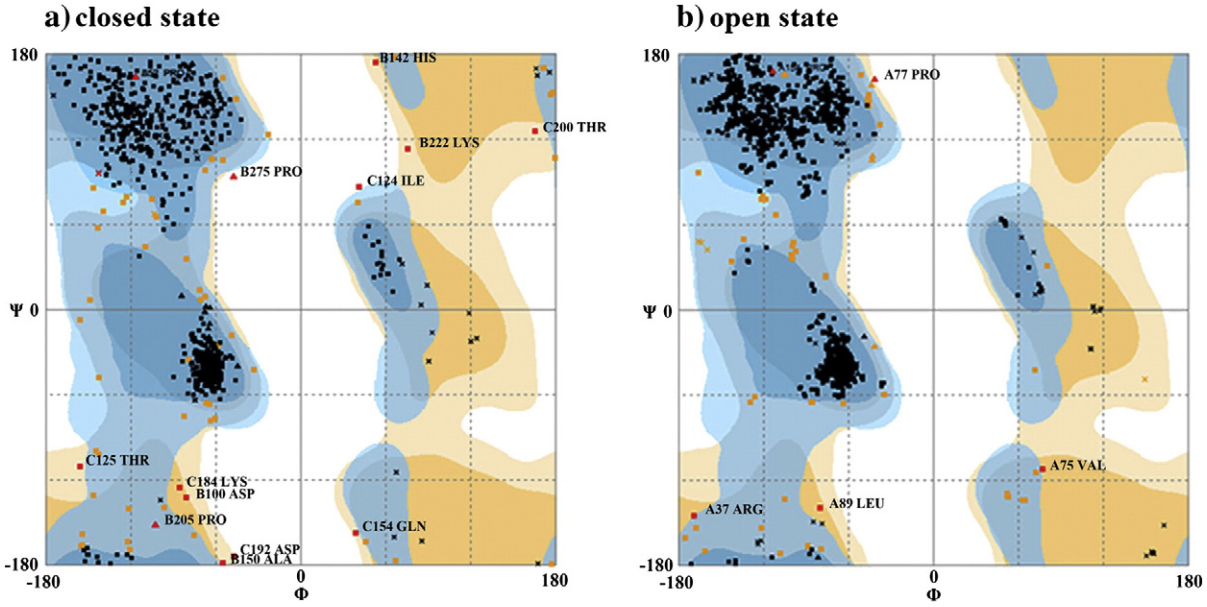

Fig. 2. Ramachandran plot of the closed-state (a) and open-state (b) $GABA_AR$: (a) A total of 93.5% of the residues are located in the favorable areas, while 5.2% of the residues reside in allowed areas. (b) A total of 95.5% of the residues fall in the favorable areas, while 4% of the residues reside in allowed areas.

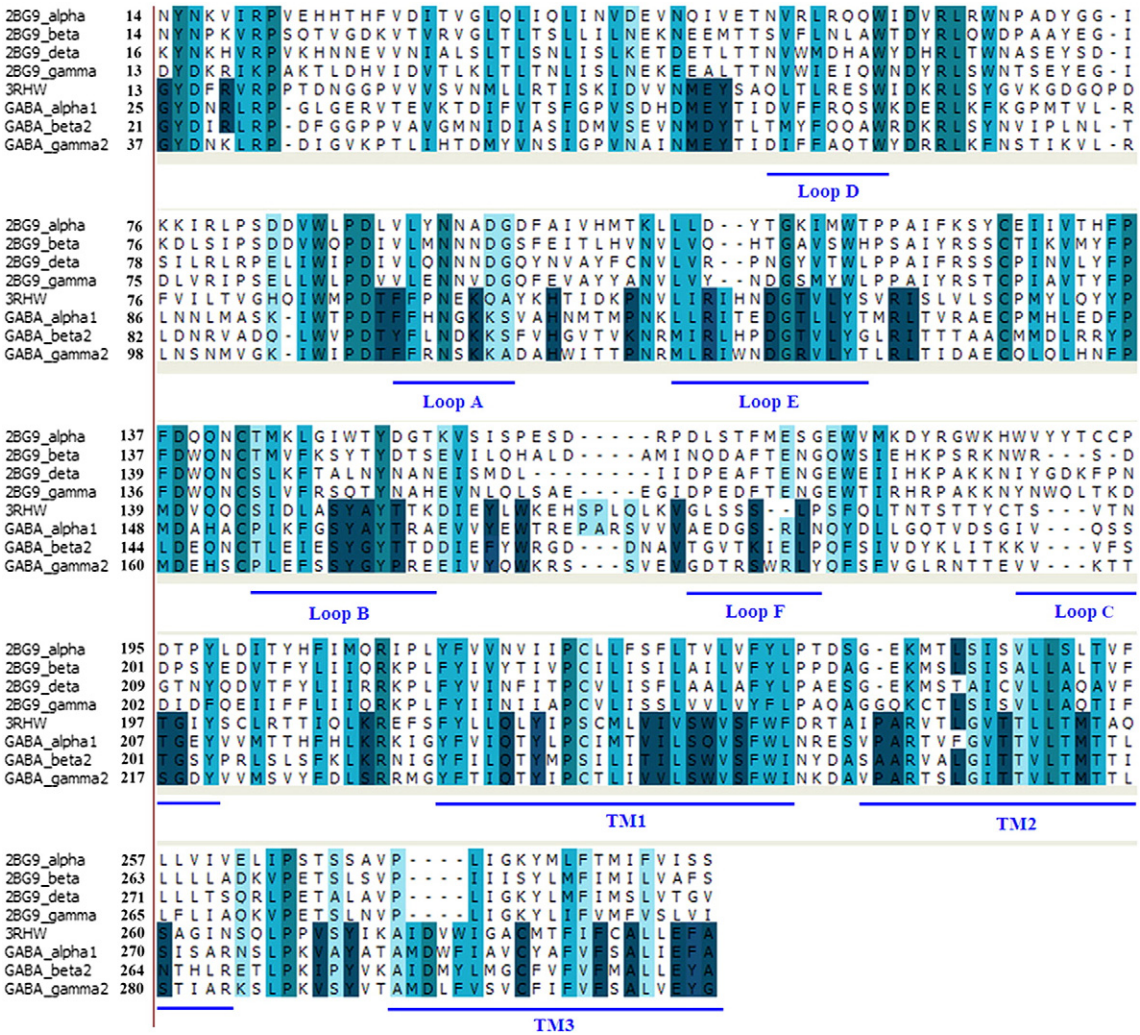

Fig. 3. Target sequences ($GABA_AR$ α_1, β_2 and γ_2 subunits) are aligned with the template sequences (GluCl and α, β, δ, and γ subunits of nAChR). A deeper color of the residues indicates the higher sequence identity.

residues are named residues 20′. Akabas et al. used disulfide bond trapping to examine the proximity and mobility of cysteines substituted for aligned $GABA_AR$ TM_2 segment channel-lining residues in resting and activated receptors [46]. With or without GABA, disulfide bonds formed at 20′ residues, suggesting that this end is more flexible than the rest of the segment. They suggested that the TM_2 segment α-helix extends beyond the predicted extracellular end of the TM_2 segment and that gating induces a conformational change in and/or around the N-terminal half of the TM_2–TM_3 loop. Although Asn275 (α_1), Glu269 (β_2) and Lys285 (γ_2) are all ionizable residues, they have different electrical property. Asparagine and glutamine are acidic amino acids, but lysine is a basic amino acid. Therefore, it is difficult to explain the high energy barrier from electrical property.

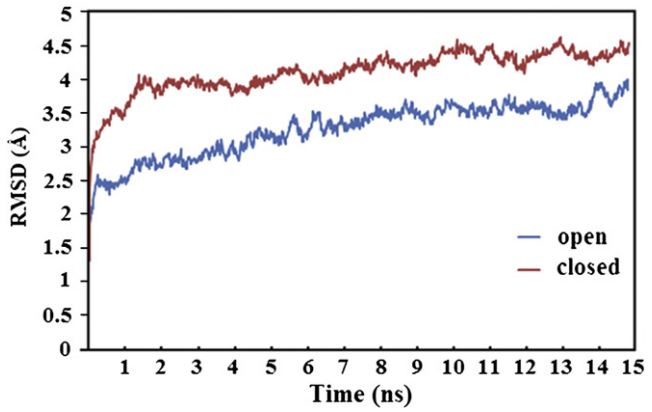

Fig. 4. Plots of RMSD with respect to time (15 ns) for the closed-state and open-state $GABA_AR$ with reference to the corresponding initial structure, demonstrating that the structures are stable.

The other energy barrier for Cl^- is formed by two Leu264 (α_1), two Leu258 (β_2) and one Leu274 (γ_2), which have been proposed as part of the hydrophobic gate in the $GABA_AR$. These residues are absolutely conserved among all known mammalian subunits of the ligand-gated ion channel superfamily and are named as the L9′ residue of TM_2 (Fig. 7). It suggests that L9′ might play an important role in pentameric ligand gated ion channels. Unwin proposed that the TM_2 in nAChR would allow the leucine side chain to project inward and associate in a tight ring via hydrophobic interactions and maintain the pore in the closed state, by bending toward the central axis [47]. When agonist binds to the receptor, the hydrophobic interactions are weakened, the TM_2 regions twist, and the pore opens. The ring of leucines constituted the gate of the pore, and that agonist binding triggered a rotation of the TM_2 segments of each subunit in the pentamer, thereby opening the channel during gating. Additionally, the study of replacing the L9′ with polar residues (Ser or Thr) to

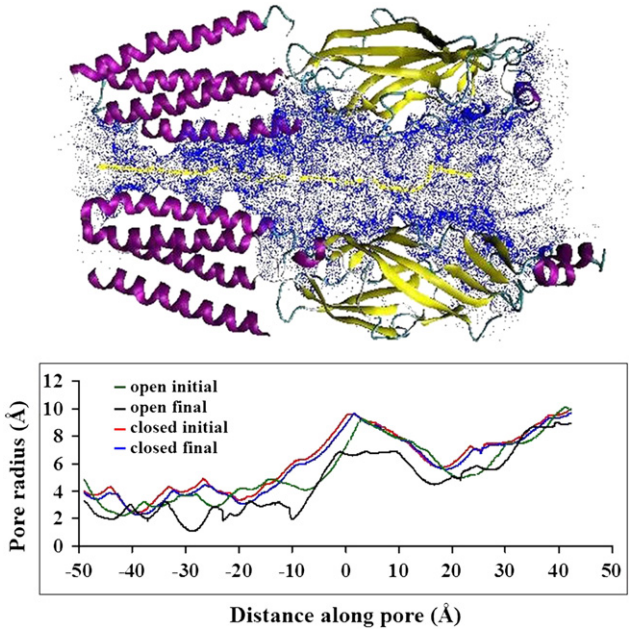

Fig. 5. Pore radius plotted as a function of position along the channel axis for the closed-channel before (red line) and after (blue line) 15 ns of MD simulations, and pore radius plotted as a function of position along the channel axis for the open-channel before (green line) and after (black line) 15 ns of MD simulations. The pore was measured by the number of dots inside the channel.

decrease apparent desensitization in $GABA_AR$ has been reported [48–50].

We examined the simulation trajectory and try to correlate the force peaks in the plot with specific events in the closed-state $GABA_AR$. A trajectory snapshot depicting the translocation of the Cl^- ion at the position 20′ with the closest pore-lining residues is shown in Fig. 8. During the simulation, the Cl^- ion moved toward the Asn275 (α_1) that surround the pore while also maintaining a close interaction with the amino group of the asparagin residue. The orientation of pore-lining hydrophobic side chains often controlled the channel opening. The residues Leu264 (α_1), Leu258 (β_2) and Leu274 (γ_2) formed the hydrophobic ring in the center of TM_2. Fig. 9 shows the side-chain orientations of residues comprising hydrophobic gate in the closed-state $GABA_AR$. It is notable that the side chains of L9′ always stretch toward the pore center, which made the pore smaller. Indeed, the Cl^- PMF for

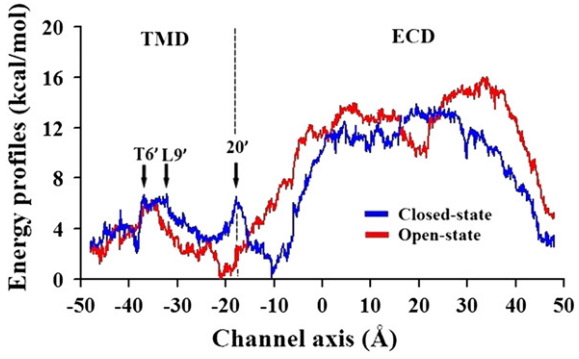

Fig. 6. Comparison of free energy profiles for transporting Cl^- through the closed-state (blue) and open-state (red) $GABA_AR$. The ECD is from $z = 48$ Å to $z = -20$ Å and the TMD is from $z = -20$ Å to $z = -48$ Å. The position of the TM_2 pore-lining residues 20′, L9′ and T6′ are labeled at the top of the graphs.

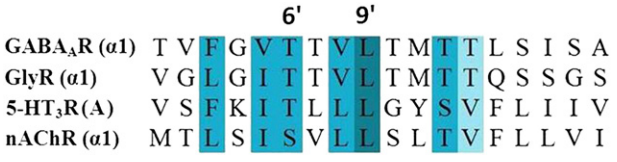

Fig. 7. Sequence alignments of the TM_2 of selected pentameric ligand gated ion channels. The sequences are retrieved from the ExPASy Molecular Biology Server, including $GABA_AR$ (α_1) (UniProt ID: P14867), GlyR (α_1) (UniProt ID: P23415), 5-HT_3R (A) (UniProt ID: P46098) and nAChR (α_1) (UniProt ID: P02708). A deeper color of the residues indicates the higher sequence identity. The residues L9′ and T6′ are labeled.

$GABA_AR$ revealed a hydrophobic restriction with a significant barrier in TM_2. Therefore, we proposed that the L9′ has the capacity to impede ion flow and the function as the putative gate of the channel.

In the TMD of the open-state $GABA_AR$, a high energy barrier with 6.1 ± 0.2 kcal/mol for Cl^- was found near the residues of T6′, including two Thr261 (α_1), two Thr255 (β_2) and one Thr271 (γ_2). We analyzed the trajectory data to observe the motion of these residues when Cl^- transporting through (Fig. 10) this region. Once the Cl^- ion passed through the position T6′, its movement was no longer confined to the channel axis.

To further investigate the ABF simulation results of the open-state and closed-state systems, we summarized the major free-energy barriers in Table 1. Comparisons between the free-energy barriers of the open-state and closed-state systems lead to the following conclusions:

1. The standard deviation for the Cl^- PMF near the excellular entrance was relatively large. This result might be due to this region was highly positively charged. And we inferred the positively charged residues Lys106 (α_1), Lys102 (β_2) and Lys118 (γ_2) play key roles. However, there still many experiments should be tested for these residues.
2. It suggested that the PMF inside the TM pore was converged fairly well. On the whole, the PMF in the TMD is lower than that in the ECD. However, our PMF calculations predicted the existence of three energy barriers for Cl^- at position L9′, T6′ and 20′ in the TMD. Ion permeation and selectivity are proposed to be determined at sites along the TMD. The residues contributed by each of the five subunits have been hypothesized to interact with permeant ions to control the magnitude of channel conductance. Through mutagenesis experiments, it has been demonstrated that channel-lining residues could significantly influence the conductance [38,44,51,52].

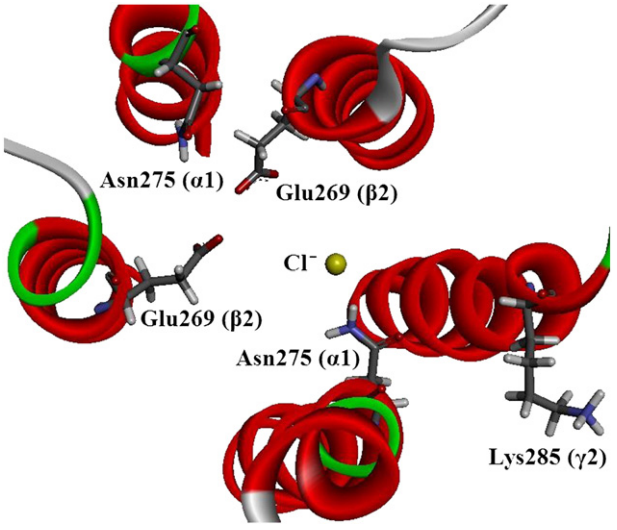

Fig. 8. Top view of the Cl^- movement in the TM_2 of the closed-state $GABA_AR$, with pore-lining side chains Asn275 (α_1), Glu269 (β_2) and Lys285 (γ_2) shown as stick representation.

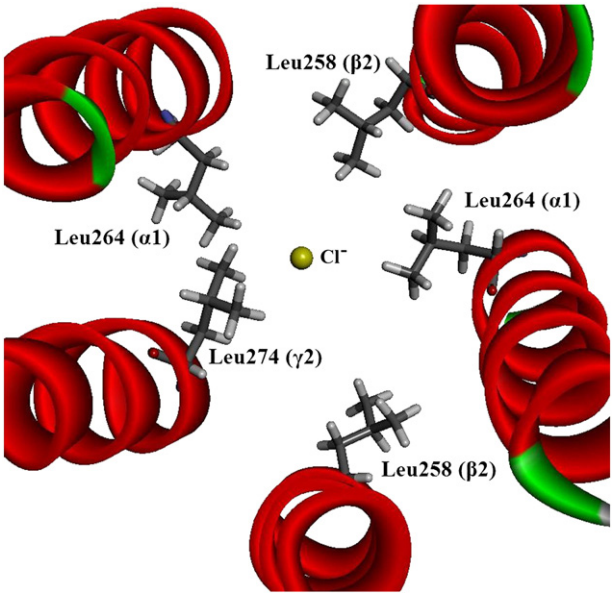

Fig. 9. Top view of the Cl^- movement in the TM_2 of the closed-state $GABA_AR$, with pore-lining hydrophobic side chains L9′ shown as stick representation.

In our study, the PMF of the TMD in the open-state $GABA_AR$ is smaller than that in the closed-state $GABA_AR$. There is one energy barrier for open-state $GABA_AR$ in the TMD. Pentameric ligand gated ion channels are associated with multiple conductances (e.g., GlyR has five distinguishable conductances) [53–55]. The conductance of the $GABA_AR$ ranged between 10 and 80 pS when exposed to low GABA concentrations [56]. It means that there are barriers in the open-state $GABA_AR$ to control the ion permeation. Otherwise the conductance would stay in the same level. Therefore, the PMF in the TMD could explain the large-range conductance of the open-state $GABA_AR$.

3. We examined other domains in $GABA_AR$ along the Cl^- ion pathway. The interface between the ligand binding domain and the TMD is a structural transition zone where β-sheets from the binding domain merge with the tops of α-helices from the pore domain. The PMF has a dramatic decline in this region, either the open-state or the closed-state channel, from 13 to 0 kcal/mol. This region may constitute a grand coupling pathway that functionally couples the ligand binding to the pore domain.
4. Pore radius has been evaluated along the pore axis. Compared with the pore radius along the axis, the energy barrier was independent of the pore radius. The PMF in the TMD was obviously less than that in the ECD, though the ECD has a larger pore radius.

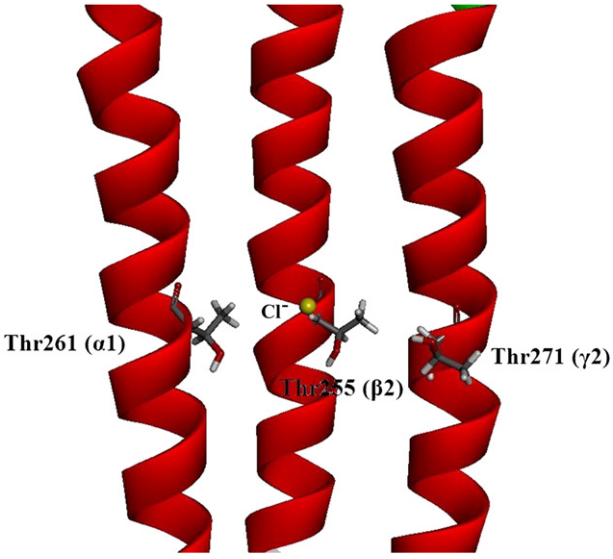

Fig. 10. View of the TM_2 in complex with Cl^-, looking parallel to the membrane, with side chains T6′ shown from three of the five TM_2 α helices.

Table 1
Free-energy barriers for Cl^- transporting through the closed-state and open-state $GABA_AR$.

Residues	Free-energy barrier (kcal/mol)	
	Closed-state	Open-state
ECD	13.0 ± 0.5	14.0 ± 0.5
T6′	6.6 ± 0.2	6.1 ± 0.2
L9′	6.7 ± 0.2	4.0 ± 0.2
20′	6.5 ± 0.2	2.5 ± 0.2

In the study of $GABA_AR$, ion permeation and selectivity are proposed to be determined at sites along the central pore in the TMD. The canonical rings of the residues contributed by each of the five subunits were hypothesized to interact with Cl^- to control the magnitude of channel conductance [57,58]. Moreover, the PMF has different end point values between cytosolic and extracellular sides, which could be remedied by a long reaction coordinate (longer than the total length of the ion channel) ABF simulation. However, it would spend much more CPU time.

In our study, the single-ion approach was used to establish a connection with experimental observations of conductance. This method has been widely used for studying ion channels [42,59,60]. According to the single-ion Nernst–Planck diffusion pore theory, strict single-ion permeation is valid only at low and moderate ion concentration [61]. At high concentration, the pore maybe occupied by more than one ion, yet the single-ion PMF will reveal much about the function of ion channels. The calculations of single-ion permeation might aim only to provide rough order of magnitude estimates. Thus, designing a theoretical framework able to rigorously extend the simulation time-scale to calculate ion fluxes is one of the most important goals in computational studies of ion channels.

4. Conclusions

In the absence of a crystal structure of $GABA_AR$, we constructed the 3D models of the closed-state and open-state human $\alpha_1\beta_2\gamma_2$ $GABA_AR$. Molecular dynamics simulations were performed for each model. Finally, two stable ion channels were obtained. Not only did the conformations of the two models change, but the charge distribution of the two models also changed dramatically. Our results suggest that ion selectivity in $GABA_AR$ was largely determined by two regions of positively charged residues positioned at the entrance and exit of the channel pore that favor or disfavor the passage of ions based on the charge. Using the MD simulations, we obtained stabilized models and analyzed the ESP, flexibility and pore radius of the $GABA_AR$ structure. Based on this information, we were able to further determine the basis of the ion selectivity and the location of ligand binding site.

In the present study, computationally demanding ABF simulations were carried out to investigate structural mechanisms of Cl^- ion translocation in the $GABA_AR$. The energy barriers are different between ECD and TMD in single ion PMF within the standard deviations of the calculations. Our results demonstrate the ECD has higher PMF than that in TMD. We identified two major energy barriers that determine the ion gating in the TMD of the closed-state $GABA_AR$, including the residues located at the position L9′ and the position 20′. We observed multiple conformations of the side chains of 20′ in ABF simulation. Nevertheless, it is clear from these results that Asn275 (α_1) is intimately involved with mechanisms directing the permeation of ions through the $GABA_AR$. In the open-state channel, pore lining residues T6′ was observed to

coordinate the permeation of Cl^- through this path, and thus mutations of these residues may assist in assessing the role of this pathway in Cl^- transport. Additionally, even though the TMD of the receptor appears more constrictive than ECD, the energetic barrier for Cl^- transporting through the TMD is smaller than that in the ECD.

In the absence of an experimentally determined structure of the $\alpha_1\beta_2\gamma_2$ $GABA_AR$, our model will be valuable for further biochemical and pharmacological studies of the detailed structure of the protein and other subtypes of $GABA_A$Rs.

Acknowledgments

We greatly appreciate the helpful discussions from Dr. Myles H. Akabas, Ph. D (Albert Einstein College of Medicine of Yeshiva University), Dr. Werner Sieghart, Ph. D (Medical University of Vienna) and Dr. Randy Bin Lin (Baylor College of Medicine).

Appendix A. Supplementary data

Supplementary data to this article can be found online at http://dx.doi.org/10.1016/j.bpc.2013.05.004.

References

[1] D.B. Pritchett, H. Sontheimer, B.D. Shivers, S. Ymer, H. Kettenmann, P.R. Schofield, P.H. Seeburg, Importance of a novel $GABA_A$ receptor subunit for benzodiazepine pharmacology, Nature 338 (1989) 582–585.
[2] W. Sieghart, G. Sperk, Subunit composition, distribution and function of GABA(A) receptor subtypes, Current Topics in Medicinal Chemistry 2 (2002) 795–816.
[3] W. Sieghart, Subunit composition and structure of GABAA-receptor subtypes, in: S.J. Enna, H. Möhler (Eds.), The GABA Receptors, Humana Press, 2007, pp. 69–86.
[4] N.L. Absalom, P.R. Schofield, T.M. Lewis, Pore structure of the Cys-loop ligand-gated ion channels, Neurochemical Research 34 (2009) 1805–1815.
[5] G.A. Johnston, GABA(A) receptor channel pharmacology, Current Pharmaceutical Design 11 (2005) 1867–1885.
[6] A.K. Mehta, M.K. Ticku, An update on $GABA_A$ receptors, Brain Research Reviews 29 (1999) 196–217.
[7] P.A. Davies, M.C. Hanna, T.G. Hales, E.F. Kirkness, Insensitivity to anaesthetic agents conferred by a class of $GABA_A$ receptor subunit, Nature 385 (1997) 820–823.
[8] E.R. Korpi, S.T. Sinkkonen, $GABA_A$ receptor subtypes as targets for neuropsychiatric drug development, Pharmacology and Therapeutics 109 (2006) 12–32.
[9] U. Rudolph, F. Crestani, H. Möhler, GABAA receptor subtypes: dissecting their pharmacological functions, Trends in Pharmacological Sciences 22 (2001) 188–194.
[10] I. Sarto-Jackson, W. Sieghart, Assembly of GABAA receptors (Review), Molecular and Membrane Biology 25 (2008) 302–310.
[11] V. Campagna-Slater, D.F. Weaver, Molecular modelling of the $GABA_A$ ion channel protein, Journal of Molecular Graphics and Modelling 25 (2007) 721–730.
[12] J. Cheng, X.-L. Ju, Homology modeling and atomic level binding study of $GABA_A$ receptor with novel enaminone amides, European Journal of Medicinal Chemistry 45 (2010) 3595–3600.
[13] T. Sander, B. Frølund, A.T. Bruun, I. Ivanov, J.A. McCammon, T. Balle, New insights into the $GABA_A$ receptor structure and orthosteric ligand binding: receptor modeling guided by experimental data, Proteins 79 (2011) 1458–1477.
[14] J.R. Trudell, E. Bertaccini, Comparative modeling of a GABAA alpha1 receptor using three crystal structures as templates, Journal of Molecular Graphics and Modelling 23 (2004) 39–49.
[15] E.J. Haddadian, M.H. Cheng, R.D. Coalson, Y. Xu, P. Tang, In silico models for the human alpha4beta2 nicotinic acetylcholine receptor, The Journal of Physical Chemistry. B 112 (2008) 13981–13990.
[16] F. Zhu, G. Hummer, Pore opening and closing of a pentameric ligand-gated ion channel, Proceedings of the National Academy of Sciences of the United States of America 107 (2010) 19814–19819.
[17] Y. Zhang, G.A. Voth, Combined metadynamics and umbrella sampling method for the calculation of ion permeation free energy profiles, Journal of Chemical Theory and Computation 7 (2011) 2277–2283.
[18] E. Darve, D. Rodriguez-Gomez, A. Pohorille, Adaptive biasing force method for scalar and vector free energy calculations, Journal of Chemical Physics 128 (2008) 144120.
[19] E. Darve, A. Pohorille, Calculating free energies using average force, Journal of Chemical Physics 115 (2001) 9169–9183.
[20] J. Hénin, C. Chipot, Overcoming free energy barriers using unconstrained molecular dynamics simulations, Journal of Chemical Physics 121 (2004) 2904–2914.
[21] G.M. Torrie, J.P. Valleau, Nonphysical sampling distributions in Monte Carlo free-energy estimation: umbrella sampling, JCoPh 23 (1977) 187–199.
[22] I. Ivanov, X. Cheng, S.M. Sine, J.A. McCammon, Barriers to ion translocation in cationic and anionic receptors from the Cys-loop family, Journal of the American Chemical Society 129 (2007) 8217–8224.
[23] S. Furini, C. Domene, Selectivity and permeation of alkali metal ions in K^+-channels, Journal of Molecular Biology 409 (2011) 867–878.
[24] M.H. Cheng, R.D. Coalson, Molecular dynamics investigation of Cl^- and water transport through a eukaryotic CLC transporter, Biophysical Journal 102 (2012) 1363–1371.
[25] F. Zhu, G. Hummer, Theory and simulation of ion conduction in the pentameric GLIC channel, Journal of Chemical Theory and Computation 8 (2012) 3759–3768.
[26] R.E. Hibbs, E. Gouaux, Principles of activation and permeation in an anion-selective Cys-loop receptor, Nature 474 (2011) 54–60.
[27] C.N. Connolly, K.A. Wafford, The Cys-loop superfamily of ligand-gated ion channels: the impact of receptor structure on function, Biochemical Society Transactions 32 (2004) 529–534.
[28] M.L. Jensen, A. Schousboe, P.K. Ahring, Charge selectivity of the Cys-loop family of ligand-gated ion channels, Journal of Neurochemistry 92 (2005) 217–225.
[29] D. Eramian, M.Y. Shen, D. Devos, F. Melo, A. Sali, M.A. Marti-Renom, A composite score for predicting errors in protein structure models, Protein Science 15 (2006) 1653–1666.
[30] S.W. Baumann, R. Baur, E. Sigel, Forced subunit assembly in $\alpha1\beta2\gamma2$ $GABA_A$ receptors. Insight into the absolute arrangement, Journal of Biological Chemistry 277 (2002) 46020–46025.
[31] S.C. Lovell, I.W. Davis, W.B. Arendall III, P.I. de Bakker, J.M. Word, M.G. Prisant, J.S. Richardson, D.C. Richardson, Structure validation by Calpha geometry: phi, psi and Cbeta deviation, Proteins 50 (2003) 437–450.
[32] J.C. Phillips, R. Braun, W. Wang, J. Gumbart, E. Tajkhorshid, E. Villa, C. Chipot, R.D. Skeel, L. Kalé, K. Schulten, Scalable molecular dynamics with NAMD, Journal of Computational Chemistry 26 (2005) 1781–1802.
[33] R.W. Pastor, A.D. MacKerell, Development of the CHARMM force field for lipids, Journal of Physical Chemistry Letters 2 (2011) 1526–1532.
[34] G. Martyna, D. Tobias, M. Klein, Constant pressure molecular dynamics algorithms, Journal of Chemical Physics 101 (1994) 4177–4189.
[35] T. Darden, D. York, L. Pedersen, Particle mesh Ewald: an N. log(N) method for Ewald sums in large systems, Journal of Chemical Physics 98 (1993) 10089–10092.
[36] D. Rodriguez-Gomez, E. Darve, A. Pohorille, Assessing the efficiency of free energy calculation methods, Journal of Chemical Physics 120 (2004) 3563–3578.
[37] T. Luu, B. Cromer, P.W. Gage, M.L. Tierney, A role for the 2′ residue in the second transmembrane helix of the GABA A receptor gamma2S subunit in channel conductance and gating, Journal of Membrane Biology 205 (2005) 17–28.
[38] J. Horenstein, D.A. Wagner, C. Czajkowski, M.H. Akabas, Protein mobility and GABA-induced conformational changes in GABA(A) receptor pore-lining M2 segment, Nature Neuroscience 4 (2001) 477–485.
[39] O.S. Smart, J.G. Neduvelil, X. Wang, B.A. Wallace, M.S. Sansom, HOLE: a program for the analysis of the pore dimensions of ion channel structural models, Journal of Molecular Graphics 14 (1996) 354–360, (376).
[40] N.A. Baker, D. Sept, S. Joseph, M.J. Holst, J.A. McCammon, Electrostatics of nanosystems: application to microtubules and the ribosome, Proceedings of the National Academy of Sciences of the United States of America 98 (2001) 10037–10041.
[41] T.J. Dolinsky, P. Czodrowski, H. Li, J.E. Nielsen, J.H. Jensen, G. Klebe, N.A. Baker, PDB2PQR: expanding and upgrading automated preparation of biomolecular structures for molecular simulations, Nucleic Acids Research 35 (2007) W522–W525.
[42] M.H. Cheng, R.D. Coalson, P. Tang, Molecular dynamics and brownian dynamics investigation of ion permeation and anesthetic halothane effects on a proton-gated ion channel, Journal of the American Chemical Society 132 (2010) 16442–16449.
[43] M. Moroni, J.O. Meyer, C. Lahmann, L.G. Sivilotti, In glycine and GABA(A) channels, different subunits contribute asymmetrically to channel conductance via residues in the extracellular domain, Journal of Biological Chemistry 286 (2011) 13414–13422.
[44] M. Scheller, S.A. Forman, Coupled and uncoupled gating and desensitization effects by pore domain mutations in GABA(A) receptors, Journal of Neuroscience 22 (2002) 8411–8421.
[45] L. Chen, K.A. Durkin, J.E. Casida, Spontaneous mobility of GABAA receptor M2 extracellular half relative to noncompetitive antagonist action, Journal of Biological Chemistry 281 (2006) 38871–38878.
[46] A.K. Bera, M. Chatav, M.H. Akabas, GABA(A) receptor M2–M3 loop secondary structure and changes in accessibility during channel gating, Journal of Biological Chemistry 277 (2002) 43002–43010.
[47] N. Unwin, Acetylcholine receptor channel imaged in the open state, Nature 373 (1995) 37–43.
[48] Y. Chang, D.S. Weiss, Substitutions of the highly conserved M2 leucine create spontaneously opening rho1 gamma-aminobutyric acid receptors, Molecular Pharmacology 53 (1998) 511–523.
[49] M.L. Tierney, B. Birnir, N.P. Pillai, J.D. Clements, S.M. Howitt, G.B. Cox, P.W. Gage, Effects of mutating leucine to threonine in the M2 segment of alpha1 and beta1 subunits of GABAA alpha1beta1 receptors, Journal of Membrane Biology 154 (1996) 11–21.
[50] Y. Chang, R. Wang, S. Barot, D.S. Weiss, Stoichiometry of a recombinant GABAA receptor, Journal of Neuroscience 16 (1996) 5415–5424.
[51] E.B. Gonzales, C.L. Bell-Horner, M.I. Dibas, R.Q. Huang, G.H. Dillon, Stoichiometric analysis of the TM2 6′ phenylalanine mutation on desensitization in alpha1beta2 and alpha1beta2gamma2 GABA A receptors, Neuroscience Letters 431 (2008) 184–189.
[52] Y. Chang, D.S. Weiss, Allosteric activation mechanism of the alpha 1 beta 2 gamma 2 gamma-aminobutyric acid type A receptor revealed by mutation of the conserved M2 leucine, Biophysical Journal 77 (1999) 2542–2551.
[53] J. Bormann, H. Kettenmann, Patch-clamp study of gamma-aminobutyric acid receptor Cl^- channels in cultured astrocytes, Proceedings of the National Academy of Sciences of the United States of America 85 (1988) 9336–9340.
[54] J.W. Lynch, Molecular structure and function of the glycine receptor chloride channel, Physiological Reviews 84 (2004) 1051–1095.

[55] J.A. Peters, M.A. Cooper, J.E. Carland, M.R. Livesey, T.G. Hales, J.J. Lambert, Novel structural determinants of single channel conductance and ion selectivity in 5-hydroxytryptamine type 3 and nicotinic acetylcholine receptors, The Journal of Physiology 588 (2010) 587–596.
[56] S. Gaul, N. Ozsarac, L. Liu, R.H. Fink, P.W. Gage, The neuroactive steroids alphaxalone and pregnanolone increase the conductance of single GABAA channels in newborn rat hippocampal neurons, The Journal of Steroid Biochemistry and Molecular Biology 104 (2007) 35–44.
[57] S.B. Hansen, H.L. Wang, P. Taylor, S.M. Sine, An ion selectivity filter in the extracellular domain of Cys-loop receptors reveals determinants for ion conductance, Journal of Biological Chemistry 283 (2008) 36066–36070.
[58] M.L. Jensen, L.N. Pedersen, D.B. Timmermann, A. Schousboe, P.K. Ahring, Mutational studies using a cation-conducting GABAA receptor reveal the selectivity determinants of the Cys-loop family of ligand-gated ion channels, Journal of Neurochemistry 92 (2005) 962–972.
[59] Y. Luo, B. Egwolf, D.E. Walters, B. Roux, Ion selectivity of alpha-hemolysin with a beta-cyclodextrin adapter. I. Single ion potential of mean force and diffusion coefficient, The Journal of Physical Chemistry. B 114 (2010) 952–958.
[60] P. Akhshi, G. Acton, G. Wu, Molecular dynamics simulations to provide new insights into the asymmetrical ammonium ion movement inside of the [d(G3T4G4)]2G-quadruplex DNA structure, The Journal of Physical Chemistry. B 116 (2012) 9363–9370.
[61] P. McGill, M.F. Schumaker, Boundary conditions for single-ion diffusion, Biophysical Journal 71 (1996) 1723–1742.